Robotica (2007) volume 25, pp. 367–374. © 2007 Cambridge University Press
doi:10.1017/S0263574706003183 Printed in the United Kingdom

Robust control of underactuated bipeds using sliding modes

Mehdi Nikkhah†, Hashem Ashrafiuon†,* and Farbod Fahimi‡

†*Department of Mechanical Engineering, Villanova University, Villanova, PA 19085, USA*
‡*Department of Mechanical Engineering, University of Alberta, Edmonton, Alberta T6G 2G8, Canada*

(Received in Final Form: November 15, 2006. First published online: January 1, 2007)

SUMMARY

The purpose of this paper is to present a robust tracking control algorithm for underactuated biped robots capable of self-balancing in the presence of external disturbances. The biped is modeled as a five-link planar robot with four actuators located at hip and knee joints. A sliding mode control law has been developed for the biped to follow a human-like gait trajectory while keeping the torso nearly upright. The control forces are calculated by defining four first-order sliding surfaces as a linear combination of the torso and the four joint tracking errors. The control approach is shown to guarantee that all trajectories will reach and stay on these surfaces during each step, while the walking cycle stability is maintained through a Lyapunov function. The criteria for asymptotic stability of the surfaces are presented and a numerical search method is implemented for the selection of the corresponding surface parameters. The paper further investigates the robustness of the controller in response to disturbances. Numerical simulations demonstrate the tracking stability of the biped's multistep walk and its human-like response to an external disturbance.

KEYWORDS: Biped robots; Underactuated systems; Sliding mode control; Stability analysis.

1. Introduction

Bipedal walking reveals many challenging issues despite the continuously increasing research for legged locomotion. The complexity of this class of mechanical systems makes their study and design very difficult [1–4].

One of the challenges in bipedal walking is development of an efficient and robust control algorithm that ensures both stability of walking and accurate trajectory following. Researchers have used nonlinear approaches such as feedback linearization [5], sliding mode control [6–9], and computed torque method [10]. However, their focus has been control of fully actuated bipeds, where there is an actuator for each degree of freedom (DOF). In the case of underactuated robots, the reduction of the number of the actuators has the advantage of reducing the energy expenditure, simplified design, and potential use for spinal or leg injury rehabilitation purposes. However, the control problem and stability analysis become more difficult.

The method of Poincare has been used to study the stability of underactuated biped motion in several studies. As an example researchers have studied and verified the convergence of motion into a cyclic trajectory in a compass biped model based on numerical computation of Poincare map [11]. This method has been used to study the stability of a simple passive biped without torso. As the dimension of the model increases, the stability analysis, using standard Poincare map, becomes impractical due to its complexity. However, in ref. [12], the stability analysis of a 3-DOF biped has been investigated with reduction of the Poincare map to numerical calculation of a one-dimensional problem. This new approach has been implemented in ref. [13] to control a 5-DOF biped. In ref. [14], it has been assumed that the biped follows the desired motion based on controller development as in ref. [12] and its stability has been investigated through dynamics of the shin angle with a one-dimensional Poincare map. This paper studies the stability of the motion during the complete walking cycle. In ref. [15], a second-order sliding mode control has been developed to control the walking of a 5-DOF biped with four actuators. This work is the continuation of the authors' previous works [12], [13], where the stability proof is based on the Poincare method. These approaches encode the walking pattern to posture conditions and reduce the dimension of the control problem effectively rendering it into a fully actuated one by introducing a set of output functions to control the torso, hip, and swing leg end.

An alternative approach has been proposed where the geometric evolution of the bipedal configuration is controlled and not the temporal evolution [16], [17]. In these works, the stability of the control law has been investigated through angular momentum of the biped about the contact point during the single support phase (SSP). The method also reduces the control problem into a fully actuated one by introducing a virtual time-dependent input and assumes no modeling error or disturbances. In ref. [16], optimized reference trajectories are tracked with the help of a time-scaling control. In ref. [17], the reference trajectory is defined for five generalized coordinates as a function of a scalar path parameter that is varying between 0 and 1. This parameter is dependant on the dynamics of the biped. In ref. [18], partial feedback linearization method has been used to control the entire walking cycle including the double support phase (DSP). The stability of the SSP and DSP have been investigated through development of a Lyapunov function along the trajectory and the impact phase has been treated as external perturbation. The torso motion stability proof for this method relies on an accurate dynamic model and cancellation of the nonlinear terms. Other methods include

* Corresponding author. E-mail: hashem.ashrafiuon@villanova.edu

linearization-based approaches that may have the advantage of integrating actuator saturation into the control law [19].

The main objective of this paper is to propose a stable and robust control law for a 5-DOF biped with four actuators located at hip and knee joints [20]. The goal is to stabilize the torso while lower body follows a desired walking profile. The control law is derived based on sliding mode control approach. Four first-order linear sliding surfaces are defined in terms of the torso and the four joint position and velocity tracking errors, leading to the derivation of the four controllers.

The stability of the control law can be explained in terms of the reaching and sliding phases of the sliding mode approach. The walking cycle was proven to be stable since the impact at the end of each step introduces a jump that throws the trajectory off the intersection of the surfaces. The standard Lyapunov function in sliding mode control, however, pushes the trajectory back on the surfaces in finite time. During the sliding phase, the system dynamics is represented by the four linear first-order surfaces and one nonlinear equation derived through a simple partial feedback linearization process. Since the biped is linearly controllable [21], the stability criteria are derived based on linearization of the one nonlinear equation. Consequently, we have used a combination of symbolic manipulation and a numerical search method to determine the surface parameters in the stable region.

Our approach has either one or both of the following two advantages over the existing methods. First, sliding mode control approach guarantees stability in the presence of significant but bounded modeling uncertainties and disturbances. Second, the joint trajectories are directly controlled rather than a transformed set of output functions that define the motion of the biped's feet and hip. This provides additional flexibility for choosing an energy-efficient desired walking trajectory.

2. Biped Model

2.1. Kinematic model

We present a sagittal model of an anthropomorphic biped in xy plane, as shown in Fig. 1. The model consists of five rigid links, a torso, and two identical legs, each having two links connected via knee joints. Two coaxial hip joints connect the legs to torso and each joint has one rotary DOF. The biped in the SSP can be considered as a 5-DOF biped whose model is represented by four relative joint angles and the torso absolute angle. Biped motion is controlled by four actuators located at knee and hip joints. Hence, it is categorized as an underactuated system in the SSP.

2.2. Dynamic model

Based on the assumption that the DSP is instantaneous, the dynamic model can be described in two parts, which consists of the SSP and an impact model.

2.2.1. Single support phase model. During the SSP, the connection between the stance leg and the ground is modeled as a pivot joint. The equations of motion may be written as

$$\mathbf{D}(\mathbf{q})\ddot{\mathbf{q}} + \mathbf{C}(\mathbf{q}, \dot{\mathbf{q}}) + \mathbf{G}(\mathbf{q}) = \mathbf{U}, \tag{1}$$

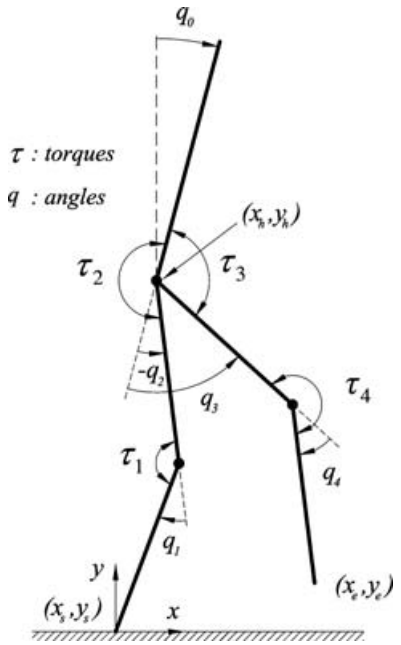

Fig. 1. Configuration variables of 5-DOF biped.

where $\mathbf{q} = [q_1, q_2, q_3, q_4, q_0]^{\mathrm{T}}$ is the vector of generalized coordinates, $\mathbf{U} = [\boldsymbol{\tau}^{\mathrm{T}}, 0]^{\mathrm{T}}$, $\boldsymbol{\tau} = [\tau_1, \tau_2, \tau_3, \tau_4]^{\mathrm{T}}$ vector of actuator forces, $\mathbf{D} \in \Re^{(5\times5)}$ the inertia matrix, and $\mathbf{C}$ and $\mathbf{G} \in \Re^{(5\times1)}$ vectors of centrifugal and coriolis terms and gravity terms, respectively.

2.2.2. Impact model. Impact occurs when the swing leg of the biped touches the ground, which we have modeled as contact between two rigid bodies. At this moment, the roles of the swing and the stance legs are exchanged. The basic assumptions for impact modeling are: the external forces on the biped can be represented by impulsive forces, a discontinuity occurs in the joint velocities due to rigid body contact, positions remain unchanged and continuous, and the actuator torques are not impulsional. Formulation of the impact model requires the assumption that at the moment when the free leg touches the ground, the stance leg immediately leaves the ground. Therefore, contact between the swing leg and the ground is modeled as a pivot joint connection. Further, we must use a 7-DOF model that allows the free motion of the stance leg [6]. Hence, we need to add the Cartesian coordinate of the stance leg end (x_s, y_s) to the generalized coordinates:

$$\mathbf{q}_C = [q_1, q_2, q_3, q_4, q_0, x_s, y_s]^{\mathrm{T}}. \tag{2}$$

The equations of motion for the impact duration can be written as

$$\mathbf{D}_C(\mathbf{q}_C)\ddot{\mathbf{q}}_C + \mathbf{C}_C(\mathbf{q}_C, \dot{\mathbf{q}}_C) + \mathbf{G}_C(\mathbf{q}_C) = \mathbf{U}_C + \mathbf{F}_\delta, \tag{3}$$

where $\mathbf{D}_C \in \Re^{(7\times7)}$, $\mathbf{C}_C, \mathbf{G}_C \in \Re^{(7\times1)}$, $\mathbf{U}_c = [\boldsymbol{\tau}^{\mathrm{T}}, 0, 0, 0]^{\mathrm{T}}$, and $\mathbf{F}_\delta \in \Re^{(7\times1)}$ is the generalized constraint force. Integration of Eq. (3) over an infinitesimal duration of impact ($[t_0, t_0 + \Delta t]$, $\Delta t \to 0$) leads to the expression of conservation of

https://doi.org/10.1017/S0263574706003183 Published online by Cambridge University Press

momentum about the contact point [6]

$$\mathbf{D}_{\mathrm{C}}(\mathbf{q}_{\mathrm{C}})(\dot{\mathbf{q}}_{\mathrm{C}}^{+} - \dot{\mathbf{q}}_{\mathrm{C}}^{-}) = \int_{t_0}^{t_0+\Delta t} \mathbf{F}_{\delta} \,.\, \mathrm{d}t, \tag{4}$$

where $\dot{\mathbf{q}}_{\mathrm{C}}^{-}$ and $\dot{\mathbf{q}}_{\mathrm{C}}^{+}$ denote the joint velocities just before and after the impact. Assuming that the external forces are acting only at the end of the swing leg (as the stance leg detaches from the ground immediately), one may write the generalized constraint forces as

$$\mathbf{F}_{\delta} = \mathbf{J}^{T}\boldsymbol{\lambda}, \tag{5}$$

where $\mathbf{J} \in \Re^{(2\times 7)}$ represents the Jacobian of the Cartesian position of the swing leg end $(x_{\mathrm{s}}, y_{\mathrm{s}})$ with respect to $\mathbf{q}_{\mathrm{C}}$ and $\boldsymbol{\lambda} \in \Re^{(2\times 1)}$ denotes Cartesian force vector acting on the swing leg end during impact. Assuming that the swing leg does not slip or rebound, we can also write

$$\mathbf{J}\dot{\mathbf{q}}_{\mathrm{C}}^{+} = \mathbf{0}. \tag{6}$$

Equations (4)–(6) provide nine linear simultaneous equations that can be solved for the angular velocities just after impact and the external forces on the swing leg end. The solution helps us determine the amount of friction required to avoid slipping and facilitates the initialization of the biped model for the next step,

$$\dot{\mathbf{q}}_{\mathrm{C}}^{+} = \dot{\mathbf{q}}_{\mathrm{C}}^{-} + \mathbf{I}(\mathbf{q}_{\mathrm{C}})(-\dot{\mathbf{x}}_{\mathrm{e}}^{-}), \tag{7}$$

where $\mathbf{I}(\mathbf{q}_{\mathrm{C}}) = \mathbf{D}_{\mathrm{C}}^{-1}\mathbf{J}^{\mathrm{T}}(\mathbf{J}\mathbf{D}_{\mathrm{C}}^{-1}\mathbf{J}^{\mathrm{T}})^{-1}$ and $\dot{\mathbf{x}}_{\mathrm{e}}^{-}$ denotes the velocity of the swing leg end just before the impact.

3. Reference Trajectories

We define the desired trajectories based on human walking observation [13] through five constraint equations. First, the horizontal position of the swing leg end, x_{e}, is defined as a fifth-order polynomial of time

$$x_{\mathrm{e}}(t) = a_0 + a_1 t + a_2 t^2 + a_3 t^3 + a_4 t^4 + a_5 t^5, \tag{8}$$

where coefficients a_i, $i = 0, \ldots, 5$, are derived based on the desired horizontal initial and final positions, velocities, and accelerations of the swing leg end

$$\begin{aligned} x_{\mathrm{e}}(t_0) &= -L \;\; \dot{x}_{\mathrm{e}}(t_0) = v_0; \; \ddot{x}_{\mathrm{e}}(t_0) = 0 \\ x_{\mathrm{e}}(t_{\mathrm{f}}) &= L; \quad \dot{x}_{\mathrm{e}}(t_{\mathrm{f}}) = v_{\mathrm{f}}; \; \ddot{x}_{\mathrm{e}}(t_{\mathrm{f}}) = 0. \end{aligned} \tag{9}$$

Then, the vertical position of the swing leg, y_{e}, is defined as a parabolic function of x_{e}

$$y_{\mathrm{e}} = c_{2\mathrm{e}} x_{\mathrm{e}}^2 + c_{1\mathrm{e}} x_{\mathrm{e}} + c_{0\mathrm{e}}. \tag{10}$$

The coefficients of the parabola can be determined based on step length, L, and maximum height, H, i.e.,

$$c_{2\mathrm{e}} = -4H/L^2; \qquad c_{1\mathrm{e}} = 0; \qquad c_{0\mathrm{e}} = H. \tag{11}$$

Two more constraints are added to ensure that the horizontal position of the hip is centered between the two feet and its vertical position moves on a parabolic path resembling that of the swing leg end, i.e.,

$$x_{\mathrm{h}} = x_{\mathrm{e}}/2 \tag{12}$$

$$y_{\mathrm{h}} = c_{2h} x_{\mathrm{h}}^2 + c_{1h} x_{\mathrm{h}} + c_{0h}. \tag{13}$$

Similarly, the coefficients of this second parabola can be determined based on L and maximum hip height. The fifth constraint maintains nearly vertical posture for the torso

$$q_0(t) = q_0^{\mathrm{d}}, \tag{14}$$

where q_0^{d} is a small constant angle whose value depends on the average walking speed.

Using the notation "C" for "cos" and "S" for "sin," the horizontal and vertical positions of the hip can be defined based on Fig. 1 as follows:

$$x_{\mathrm{h}} = L_2 S(q_0 + q_2) + L_1 S(q_0 + q_1 + q_2) \tag{15}$$

$$y_{\mathrm{h}} = L_2 C(q_0 + q_2) + L_1 C(q_0 + q_1 + q_2) \tag{16}$$

and those of the swing leg as

$$x_{\mathrm{e}} = x_{\mathrm{h}} + L_2 S(q_3 - q_0) + L_1 S(q_3 - q_0 - q_4) \tag{17}$$

$$y_{\mathrm{e}} = y_{\mathrm{h}} - L_2 C(q_3 - q_0) - L_1 C(q_3 - q_0 - q_4), \tag{18}$$

where L_1 and L_2 represent the lengths of tibia and femur, respectively. Equations (15)–(18), called the postural conditions, can be solved to determine the desired trajectory for the four joint coordinates

$$q_1^{\mathrm{d}}(t) = \mathrm{acos}\left[\frac{x_{\mathrm{h}}^2 + y_{\mathrm{h}}^2 - L_1^2 - L_2^2}{2L_1L_2}\right] \tag{19}$$

$$q_2^{\mathrm{d}}(t) = \mathrm{atan}\left[\frac{x_{\mathrm{h}}\left(L_2 + L_1 C q_1^{\mathrm{d}}\right) - y_{\mathrm{h}} L_1 S q_1^{\mathrm{d}}}{x_{\mathrm{h}} L_1 S q_1^{\mathrm{d}} + y_{\mathrm{h}}\left(L_2 + L_1 C q_1^{\mathrm{d}}\right)}\right] - q_0^{\mathrm{d}} \tag{20}$$

$$q_3^{\mathrm{d}}(t) = \mathrm{atan}\left[\frac{x_{\mathrm{eh}}\left(L_2 + L_1 C q_4^{\mathrm{d}}\right) - y_{\mathrm{eh}} L_1 S q_4^{\mathrm{d}}}{-x_{\mathrm{eh}} L_1 S q_4^{\mathrm{d}} + y_{eh}\left(L_2 + L_1 C q_4^{\mathrm{d}}\right)}\right] + q_0^{\mathrm{d}} \tag{21}$$

$$q_4^{\mathrm{d}}(t) = \mathrm{acos}\left[\frac{x_{\mathrm{eh}}^2 + y_{\mathrm{eh}}^2 - L_1^2 - L_2^2}{2L_1L_2}\right], \tag{22}$$

where $x_{\mathrm{eh}} = x_{\mathrm{e}} - x_{\mathrm{h}}$ and $y_{\mathrm{eh}} = y_{\mathrm{e}} - y_{\mathrm{h}}$. Reference trajectories remain continuous $(\mathbf{q}_{\mathrm{C}}^{+} = \mathbf{q}_{\mathrm{C}}^{-})$ during the impact based on assumptions made in our impact model.

4. Sliding Mode Control Formulation

The goal of sliding mode control approach is to define asymptotically stable surfaces such that all system trajectories converge to these surfaces and slide along them until reaching the origin at their intersection [22]. Since the biped model, represented by Eq. (1), is underactuated, the equations are partitioned into four actuated and one

https://doi.org/10.1017/S0263574706003183 Published online by Cambridge University Press

unactuated coordinates,

$$\begin{bmatrix} \mathbf{D}_{aa} & \mathbf{D}_{a0} \\ \mathbf{D}_{a0}^{\mathrm{T}} & D_{00} \end{bmatrix} \begin{bmatrix} \ddot{\mathbf{q}}_{\mathrm{a}} \\ \ddot{q}_0 \end{bmatrix} + \begin{bmatrix} \mathbf{f}_{\mathrm{a}} \\ f_0 \end{bmatrix} = \begin{bmatrix} \boldsymbol{\tau} \\ 0 \end{bmatrix}, \tag{23}$$

where $\mathbf{f} = [\mathbf{f}_{\mathrm{a}}^{\mathrm{T}},\ f_0]^{\mathrm{T}} = \mathbf{C} + \mathbf{G}$ and may also represent external forces and disturbances. The fifth (unactuated) equation in the set (23) is a second-order nonholonomic constraint. Hence, it is completely nonintegrable and strongly accessible such that the dimension of the reachable states is not reduced [23]. In order to derive a stable control law that relies on the structure of the system equations, we redefine the actuated accelerations as input and lump all nonlinearities into a single equation

$$\ddot{\mathbf{q}}_{\mathrm{a}} = \mathbf{u} \tag{24}$$

$$\ddot{q}_0 = -D_{00}^{-1}\left(f_0 + \mathbf{D}_{a0}^{\mathrm{T}}\mathbf{u}\right) \tag{25}$$

$$\boldsymbol{\tau} = \mathbf{D}_{a0}\ddot{q}_0 + \mathbf{D}_{aa}\mathbf{u} + \mathbf{f}_{\mathrm{a}}. \tag{26}$$

First-order linear sliding surfaces are normally defined based on weighted combination of the position and velocity tracking errors $\tilde{\mathbf{q}} = \mathbf{q} - \mathbf{q}^{\mathrm{d}}$ and $\dot{\tilde{\mathbf{q}}} = \dot{\mathbf{q}} - \dot{\mathbf{q}}^{\mathrm{d}}$. Partitioning of the tracking errors into four actuated and one unactuated, the surfaces may be defined as [24]

$$\mathbf{s} = \dot{\tilde{\mathbf{q}}}_{\mathrm{a}} + \boldsymbol{\lambda}_{\mathrm{a}}\tilde{\mathbf{q}}_{\mathrm{a}} + \boldsymbol{\alpha}_0\tilde{q}_0 + \boldsymbol{\lambda}_0\tilde{q}_0, \tag{27}$$

where $\boldsymbol{\lambda}_{\mathrm{a}} \in \Re^{(4\times4)}$ and $\boldsymbol{\alpha}_0, \boldsymbol{\lambda}_0 \in \Re^{(4\times1)}$ are the constant parameters that must be selected to ensure the asymptotic stability of the sliding surfaces. Clearly, if we choose $\boldsymbol{\lambda}_{\mathrm{a}}$ as a diagonal positive definite matrix, then the surfaces are exponentially stable as long as the torso is stable, i.e., $\tilde{q}_0 \to 0$.

The control law can be calculated by defining a candidate Lyapunov function in terms of the surfaces as

$$V(\mathbf{q}, \dot{\mathbf{q}}) = \frac{1}{2}\mathbf{s}^{\mathrm{T}}\mathbf{s} \geq 0 \tag{28}$$

Thus, we must determine the control law that satisfies $\dot{V}(\mathbf{q}, \dot{\mathbf{q}}) \leq 0$ or equivalently

$$s_i\dot{s}_i \leq -\eta_i|s_i| \qquad i = 1\ldots4, \quad \eta_i > 0. \tag{29}$$

The equations considered earlier represent the reaching conditions for the four surfaces. Substituting from Eqs. (24), (25), and (27) into Eq. (29) and adding the robustness terms, one may write [20]

$$\mathbf{u} = \hat{\mathbf{M}}^{-1}\left[\boldsymbol{\alpha}_0\hat{D}_{00}^{-1}\hat{f}_0 - \dot{\mathbf{s}}_{\mathrm{r}} - \mathbf{k}\mathrm{sgn}(\mathbf{s})\right] \tag{30}$$

where "$\hat{}$" denotes that the terms are evaluated based on the estimated dynamic parameters of the system and

$$\hat{\mathbf{M}} = \mathbf{I}_4 - \boldsymbol{\alpha}_0\hat{D}_{00}^{-1}\hat{\mathbf{D}}_{a0}^{\mathrm{T}} \tag{31}$$

$$\dot{\mathbf{s}}_r = -\ddot{\mathbf{q}}_{\mathrm{a}}^{\mathrm{d}} - \boldsymbol{\alpha}_0\ddot{q}_0^{\mathrm{d}} + \boldsymbol{\lambda}_{\mathrm{a}}\dot{\tilde{\mathbf{q}}}_{\mathrm{a}} + \boldsymbol{\lambda}_0\tilde{q}_0 \tag{32}$$

$$\mathbf{k}\mathrm{sgn}(\mathbf{s}) = [k_1\mathrm{sgn}(s_1), \ldots, k_4\mathrm{sgn}(s_4)]^{\mathrm{T}}, \tag{33}$$

where $\mathbf{I}_4 \in \Re^{(4\times4)}$ denotes the Identity matrix. Note that the parameters of $\boldsymbol{\alpha}_0$ must be selected such that matrix $\hat{\mathbf{M}}$ is invertible for all biped configurations.

In Eq. (30), the gains of the "sign" functions (robustness terms), $\mathbf{k}$, must be selected such that the reaching conditions (Eq. (29)) are satisfied. Assuming that the mass and geometric properties of the biped can be accurately measured, the uncertainties and disturbances can be collected in f_0 and $\mathbf{k}$ is determined as

$$\mathbf{k} = \boldsymbol{\eta} + \boldsymbol{\alpha}_0\hat{D}_{00}^{-1}F_0, \tag{34}$$

where F_0 represents the bound on our modeling uncertainty and disturbances

$$|f_0 - \hat{f}_0| \leq F_0. \tag{35}$$

The amount of effort required for the system trajectory to reach each surface is proportional to the magnitude of the corresponding element of $\mathbf{k}$.

5. Stability Analysis

The control law of Eq. (30) is asymptotically stable if we can prove: A) matrix $\hat{\mathbf{M}}$ is invertible, B) all system trajectories reach the surfaces in finite time and remain on the surface, and C) the surfaces are asymptotically stable.

5.1. Invertibility condition

The biped inertia matrix $\hat{\mathbf{D}}$ is positive definite. Thus, the elements of vector $\hat{D}_{00}^{-1}\hat{\mathbf{D}}_{a0}$ are bounded in the biped configuration space. Further, it can be shown that the determinant of $\hat{\mathbf{M}}$ is given as $1 - \hat{D}_{00}^{-1}\boldsymbol{\alpha}_0{}^{\mathrm{T}}\hat{\mathbf{D}}_{a0}$ [25]. Hence, we can simply choose the elements of $\boldsymbol{\alpha}_0$ with sufficiently large magnitudes such that $\det(\hat{\mathbf{M}}) \neq 0$.

5.2. Reaching condition

The controller of Eq. (30) ensures that all system trajectories will reach the surface and remain there since it guarantees that $\frac{1}{2}\mathbf{s}^{\mathrm{T}}\mathbf{s}$ is a Lyapunov function even in the presence of uncertainties and disturbances which were integrated in the model through Eq. (34). The trajectories will reach each surface i within the finite time of $|s_i(0)|/\eta_i$ [26]. Note that, at the end of each step there is a jump in velocities due to impact of the swing leg and ground. This causes a perturbation in the initial conditions of the next step throwing the trajectory off the surfaces. However, the stability of multistep walk is guaranteed due to the finite time reaching conditions. Clearly, the values of η_i must be large enough to ensure a smooth transition from one step to the next but small enough to avoid excessive actuator forces.

5.3. Surface exponential stability

During the sliding phase of trajectory, the closed loop system dynamics is represented by the combination of the four first-order linear surfaces in Eq. (27) in the form $\mathbf{s} = 0$ and the one unactuated acceleration equation, namely, Eq. (25), after substituting for the control law and eliminating the robustness

https://doi.org/10.1017/S0263574706003183 Published online by Cambridge University Press

term

$$\dddot{\tilde{\mathbf{q}}}_{\mathrm{a}} + \boldsymbol{\lambda}_{\mathrm{a}}\ddot{\tilde{\mathbf{q}}}_{\mathrm{a}} + \boldsymbol{\alpha}_0\ddot{\tilde{q}}_0 + \boldsymbol{\lambda}_0\dot{\tilde{q}}_0 = 0 \quad (36)$$

$$\ddot{q}_0 + \hat{D}_{00}^{-1}\left[\hat{f}_0 + \hat{\mathbf{D}}_{0a}\hat{\mathbf{M}}^{-1}\left(\boldsymbol{\alpha}_0\hat{D}_{00}^{-1}\hat{f}_0 - \dot{\mathbf{s}}_{\mathrm{r}}\right)\right] = 0, \quad (37)$$

where the system state vector is reduced to $\mathbf{x} = [\tilde{\mathbf{q}}_{\mathrm{a}}^{\mathrm{T}}, \tilde{q}_0, \dot{\tilde{q}}_0]^{\mathrm{T}}$.

It is well known that systems with isolated equilibrium points for each fixed set of inputs (i.e., systems with potential energy such as a biped) are linearly controllable [21]. Hence, we may linearize Eq. (37) about the system trajectory and torso equilibrium point to establish linear stability criteria that can guarantee local exponential stability of the nonlinear system. Substituting for $\dddot{\tilde{\mathbf{q}}}_{\mathrm{a}}$ from Eq. (36) in the linearized form of Eq. (37), one may write

$$\ddot{\tilde{q}}_0 + \mathbf{A}_{0a}\ddot{\tilde{\mathbf{q}}}_{\mathrm{a}} + A_{00}\dot{\tilde{q}}_0 + B_{00}\tilde{q}_0 = 0. \quad (38)$$

The state matrix of the linear time varying system represented by Eqs. (36) and (38), $\dot{\mathbf{x}} = \mathbf{A}(t)\mathbf{x}$, is derived as

$$\mathbf{A}(t) = \begin{bmatrix} -\boldsymbol{\lambda}_{\mathrm{a}}]_{4\times4} & [-\boldsymbol{\lambda}_0]_{4\times1} & [-\boldsymbol{\alpha}_0]_{4\times1} \\ [\mathbf{0}]_{1\times4} & 0 & 1 \\ [\mathbf{A}_{0a}]_{1\times4} & A_{00} & B_{00} \end{bmatrix}, \quad (39)$$

where each bracket's subscript denotes the submatrix size.

Exponential stability of the linear time varying system can be established if at any time $t \geq 0$, the eigenvalues of $\mathbf{A}(t)$ all have negative real parts (i.e., the matrix is negative definite), it remains bounded [26], and

$$\int_{t_0}^{\infty} \mathbf{A}^{\mathrm{T}}(t)\mathbf{A}(t)\,\mathrm{d}t < \infty. \quad (40)$$

Since time varying components of $\mathbf{A}(t)$ are functions of the periodic desired trajectories, it is clear that $\mathbf{A}(t)$ remains bounded and Eq. (40) is satisfied.

In order to determine whether or not matrix $\mathbf{A}(t)$ is negative definite, its elements were derived symbolically using MAPLE. The characteristic polynomial for the eigenvalues of matrix $\mathbf{A}(t)$ is represented in Laplace domain as

$$b_6S^6 + b_5S^5 + b_4S^4 + b_3S^3 + b_2S^2 + b_1S + b_0 = 0 \quad (41)$$

where S is the Laplace variable. The Hurwitz stability conditions result in 13 independent coefficients

$$h_1, h_2, \ldots, h_{12}, h_{13} > 0, \quad (42)$$

where

$$h_1 = b_6, \ldots, h_7 = b_0, \quad h_8 = \frac{h_2h_3 - h_1h_4}{h_2}, \ldots \quad (43)$$

The parameters in Hurwitz criteria are time varying (i.e., depend on the biped posture changes) and functions of surface parameters $\boldsymbol{\lambda}_{\mathrm{a}}$, $\boldsymbol{\alpha}_0$, and $\boldsymbol{\lambda}_0$. Thus, the condition in Eq. (42) must be checked throughout the biped walking cycle for a given set of surface parameters. Hence, a numerical algorithm was developed to check if Eq. (42) is satisfied during the whole walking cycle while searching for surface parameters. Several guidelines may be used to reduce the complexity of the parameter search. As explained earlier, we choose $\boldsymbol{\lambda}_{\mathrm{a}}$ to be a diagonal positive definite matrix, such that the surfaces become exponentially stable as long as the torso is stable (see Eq. (36)). Another condition is that all elements of $\boldsymbol{\lambda}_0$ and $\boldsymbol{\alpha}_0$ must have the same sign to achieve an exponentially stable torso motion. Further, $|\alpha_{0_i}| \gg 1$, $i = 1 \ldots 4$, is sufficient to ensure the invertibility of matrix $\hat{\mathbf{M}}$, i.e., magnitudes of the elements of $\hat{D}_{00}^{-1}\boldsymbol{\alpha}_0^{\mathrm{T}}\hat{\mathbf{D}}_{a0}$ will be much larger than 1 for all robot configurations.

Table I. Biped geometry and inertia properties.

Link	Mass (Kg)	Center of mass (m)	Moment of inertia (Kg.m^2)	Length (m)
Torso	50	0.33	7.0	0.55
Femurs	8.6	0.27	0.69	0.41
Tibias	6.4	0.24	0.44	0.40

6. Simulation Results

Consider the biped in Fig. 1 with geometric and inertia properties as listed in Table I. A length of 0.45 m, a height of 0.05 m, and a duration of 0.45 s have been selected for each step. Also, an initial horizontal hip speed of 1.0 m/s is used based on calculation of average linear momentum during one step and the torso must lean forward for a stable walking profile. We chose this value to be 5°. The following control parameters have been selected based on the criteria and the numerical search method explained in the previous section:

$$\boldsymbol{\eta} = [40, 40, 40, 40]^{\mathrm{T}} \quad (1/\mathrm{s}^2)$$

$$\boldsymbol{\lambda}_0 = [143, 143, 143, 143]^{\mathrm{T}} \quad (1/\mathrm{s})$$

$$\boldsymbol{\lambda}_{\mathrm{a}} = \mathrm{diag}[35, 7, 7, 7] \quad (1/\mathrm{s})$$

$$\boldsymbol{\alpha}_0 = [14, 14, 14, 14]^{\mathrm{T}}$$

The large value selected for λ_{a1} is due to tibia of the stance leg being the main link that keeps the biped stable while walking. Also, the values selected for η are large to ensure a quick reaching phase for the control law. In order to avoid chattering typically associated with the sliding mode control law, we have also approximated the discontinuous sign functions (sgn(**s**)) with continuous saturation functions (sat($\frac{s}{\boldsymbol{\phi}}$)) of small boundary layers

$$\boldsymbol{\phi} = [.01, .01, .01, .01]^{\mathrm{T}} \quad (1/\mathrm{s}).$$

The smallest and the largest of the 13 Hurwitz coefficients in Eq. (42) versus the torso angle are presented in Fig. 2. The discontinuities in the plots are due to impact at the end of each step and the remaining coefficients display very similar variations. Clearly, these coefficients are positive with relatively large magnitude and display a limit cycle, which ensures the stability of the walk even in case of significant variations from the reference trajectories.

https://doi.org/10.1017/S0263574706003183 Published online by Cambridge University Press

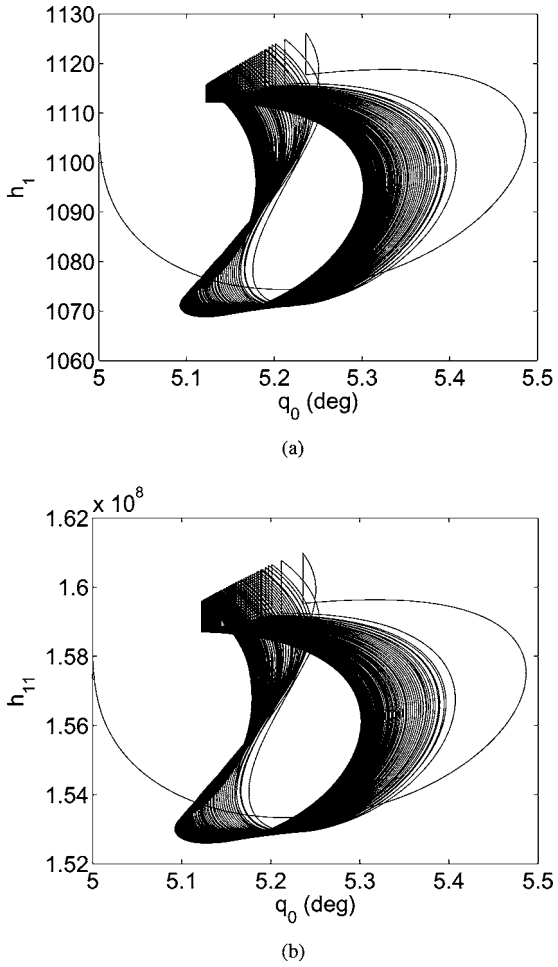

Fig. 2. Hurwitz coefficient for 120 steps; (a) h_1, (b) h_{11}.

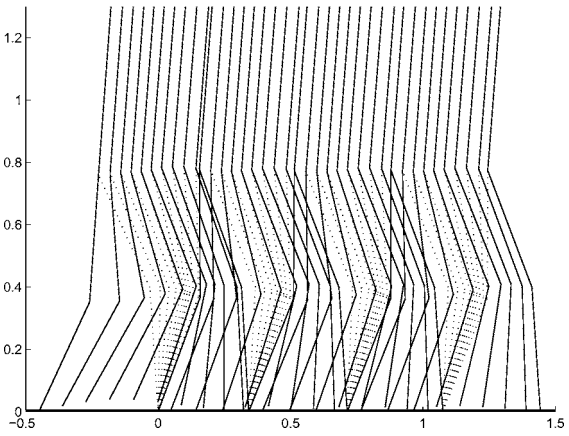

Fig. 3. Simulation of the biped for four steps, *dotted line* is the stance leg.

Figure 3 shows the biped smooth walking motion for four steps using the sliding mode control law. The phase plots of the four actuated coordinates for 120 steps demonstrate an asymptotic stability by achieving of a limit cycle, as shown in Fig. 4. Similarly, Fig. 5 shows the torso angle reaching a limit cycle in a 120-step simulation. It is clear that the controller can keep the torso near the desired angle and converges to a limit cycle with constant mean torso angle of 5.2°.

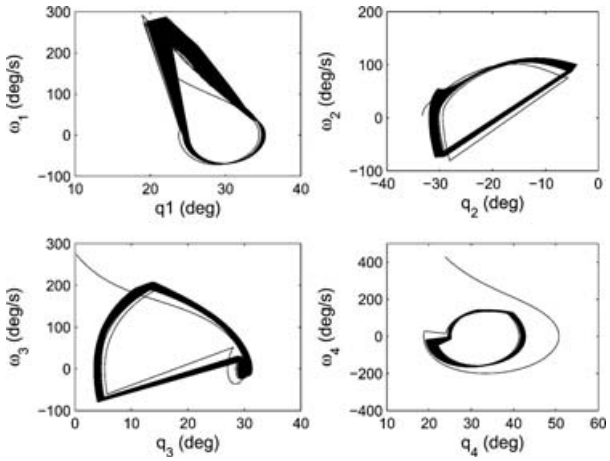

Fig. 4. Phase plots of the four actuated coordinates for 120 steps ($\omega_i \equiv \dot{q}_i$).

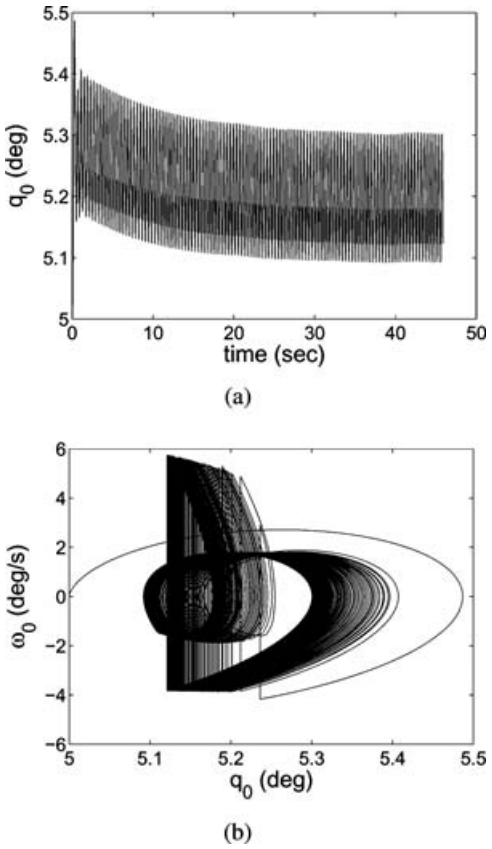

Fig. 5. Torso angle time history (a) and phase plot (b) for 120 steps ($\omega_0 \equiv \dot{q}_0$).

Figure 6 shows the required actuator torques at hip and knee joints. The actuation torque profiles are consistent with those of published results [13] and their magnitudes are very reasonable for such a large biped compared with other numerical results [19]. However, it is possible to improve these results by searching for better surface parameters through some optimal criterion [27]. Figure 7 shows the vertical and horizontal components of the ground reaction forces with maximum magnitudes of about 1000 N. and 250 N, respectively. It is clear that the vertical component of the ground reaction force is always positive and the unilateral

https://doi.org/10.1017/S0263574706003183 Published online by Cambridge University Press

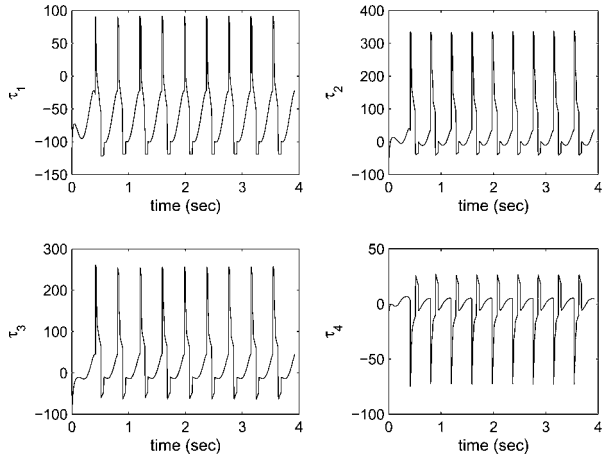

Fig. 6. Time history of the four actuator torques (N.m) for 10 steps.

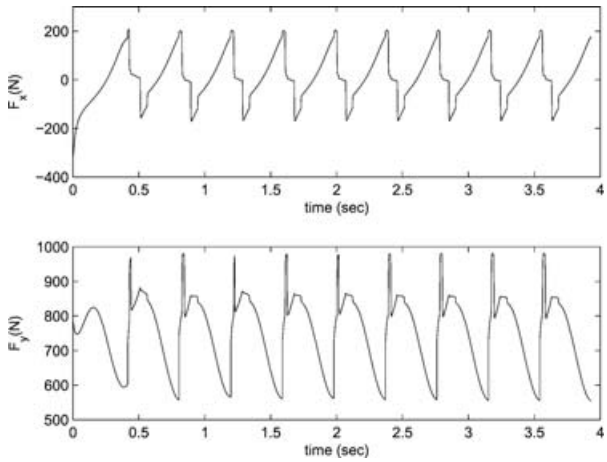

Fig. 7. Horizontal (*top*) and vertical (*bottom*) components of ground reaction forces.

constraint on the stance leg end is satisfied. Slipping will not occur as long as the friction coefficient is larger than 0.25.

Reaching and sliding phases of the sliding mode control law are demonstrated in Fig. 8 for all actuated coordinates during steps 2 and 3. As one can see, the trajectories are not on the surface at the beginning of the step due to a jump in velocities after each impact. However, the controller pushes the trajectory back on the surfaces which subsequently slide on the surfaces to the desired angles.

6.1. Response to external disturbances

An important advantage of the control law introduced in this research is its robustness with respect to external disturbances as long as its magnitude is within some known bounds. Hence, we applied an external impulsive torque of relatively large magnitude to the biped torso during its fourth step. The torque has a magnitude of 700 N.m and a duration of 0.02 s. The only knowledge of the disturbance by the controller is that its magnitude is within a limit of more than twice the actual value.

Figure 9 shows the effect of the disturbance on the torso angle during a 50-step walk. The figure demonstrates that the controller is able to recover from the "push" by the external disturbance and the torso angle reached its limit cycle with

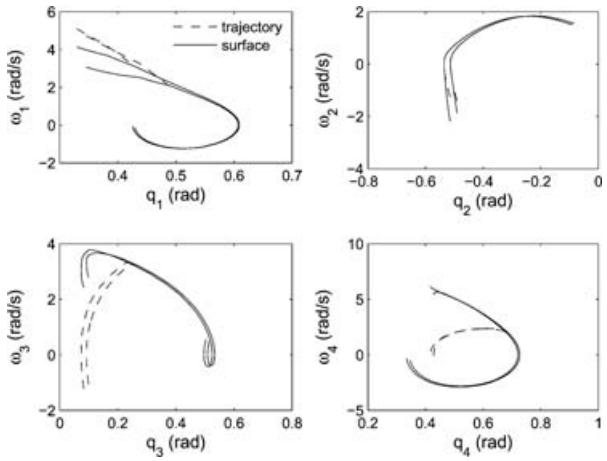

Fig. 8. Reaching and sliding phases of the control law for two steps ($\omega_i \equiv \dot{q}_i$).

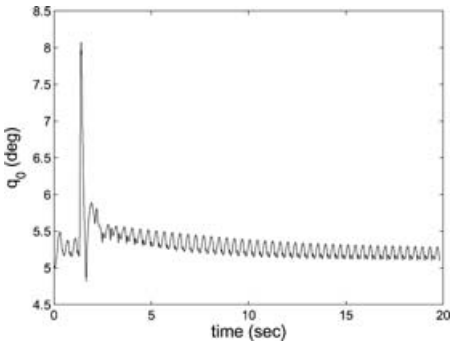

Fig. 9. Torso angle variation for 50 steps in the presence of a disturbance.

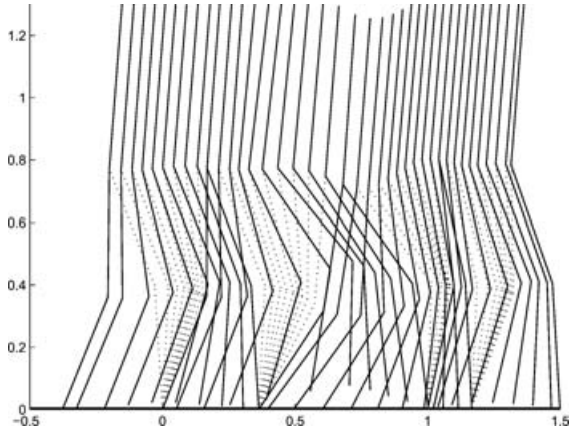

Fig. 10. Simulation of the biped motion in the presence of a disturbance.

the same constant mean angle as in the undisturbed case. Figure 10 shows the four consecutive steps before, during, and just after the application of the disturbance. The response of the biped is similar to the natural human response where the torso leans forward (pushed by the disturbance force) and immediately rotates back, while the swing leg moves up to avoid falling over.

https://doi.org/10.1017/S0263574706003183 Published online by Cambridge University Press

7. Conclusions

In this paper, the sliding mode control approach was successfully used to design a robust tracking controller for an underactuated biped. The control law was determined based on the dynamics of the biped, which was modeled as a 5-DOF system moving in the sagittal plane with four actuators located at hip and knee joints. Four first-order sliding surfaces were defined as linear combinations of the torso and the four joint tracking errors to determine the control law for the four actuators. The sliding mode control law was shown to be globally finite-time stable in the reaching phase and locally exponentially stable in the sliding phase due to linearization of one nonlinear equation in the transformed system dynamics. Symbolic manipulation and a numerical search method were used to determine the surface parameters for an asymptotically stable control law. The robustness of the controller was investigated in response to an external disturbance. It was shown that the biped is able to recover from a sudden forward push with a human-like response.

References

1. M. H. Raibert, *Legged Robots That Balance* (MIT Press, Cambridge, MA, 1986).
2. M. Vukobratovic, B. Borovac, D. Surla and D. Stokic. *Biped Locomotion* (Springer-Verlag, Berlin, Germany, 1990).
3. C. M. Chew, E. Choong, A. N. Poo and G. S. Hong, "From Science Fiction to Reality—Humanoid Robots," *International Conference on Humanoid, Nanotechnology, Information Technology, Communication and Control, Environment, and Management*, Manila, Philippines (Mar. 2003).
4. S. Lohmeier, K. Löffler, M. Gienger, H. Ulbrich and F. Pfeiffer, "Computer System and Control of Biped johnnie," *Proceedings of the IEEE International Conference on Robotics and Automation*, New Orleans, LA (Apr. 2004) pp. 4222–4227.
5. K. Mitobe, N. Mori, K. Aida and Y. Nasu, "Nonlinear Feedback Control of a Biped Walking Robot," *Proceedings of the IEEE International Conference on Robotics and Automation*, Nagoya, Japan (May 1995) pp. 2865–2870.
6. S. Tzafestas, M. H. Raibert and C. Tzafestas, "Robust sliding-mode control applied to a 5-link biped robot," *J. Intell. Robot. Syst. Theory Appl.* **15**, 67–133 (1996).
7. S. G. Tzafestas, T. E. Krikochoritis and C. S. Tzafestas, "Robust sliding-mode control of nine-link biped robot walking," *J. Intell. Robot. Syst. Theory Appl.* **20**, 375–402 (1997).
8. T. H. Chang and Y. Hurmuzlu, "Sliding control without reaching phase and its application to bipedal locomotion," *J. Dyn. Syst. Meas. Control, Trans. ASME* **115**, 447–455 (1993).
9. X. Mu and Q. Wu, "Development of a complete dynamic model of a planar five-link biped and sliding mode control of its locomotion during the double support phase," *Int. J. Control* **77**(8), 789–799 (2004).
10. B. Vanderborght, B. Verrelst, R. Van Ham and D. Lefeber, "Controlling a bipedal walking robot actuated by pleated pneumatic artificial muscles," *Robotica* **24**, 401–410 (2006).
11. A. Goswami, B. Espiau and A. Keramane, "Limit Cycles and their Stability in a Passive Bipedal Gait," *Proceedings of the IEEE International Conference on Robotics and Automation*, Minneapolis, MN (Apr. 1996) pp. 246–251.
12. J. W. Grizzle, G. Abba and F. Plestan, "Asymptotically stable walking for biped robots: Analysis via systems with impulse effects," IEEE Trans. Autom. Control **46**, 51–64 (2001).
13. F. Plestan, J. W. Grizzle, E. R. Westervelt and G. Abba, "Stable walking of a 7-DOF biped robot," IEEE Trans. Robot. Autom. **19**, 653–668 (2003).
14. S. Miossec and Y. Aoustin, "A simplified stability study for a biped walk with underactuated and overactuated phases," *Int. J. Robot. Res.* **24**, 537–551 (2005).
15. F. Plestan and S. Laghrouche, "Sliding Mode Controller for the Walking of a Biped Robot: Arbitrary Order Sliding Mode Approach," *Proceedings of the Sixth International Conference on Climbing and Walking Robots and the Support Technologies for Mobile Machines*, Catania, Italy (Sep. 2003) pp. 181–188.
16. C. Chevallereau, "Time-scaling control for an underactuated biped robot," IEEE Trans. Robot. Autom. **19**, 362–368 (2003).
17. C. Chevallereau, A. Formal'sky and D. Djoudi, "Tracking a joint path for the walk of an underactuated biped," *Robotica* **22**, 15–28 (2004).
18. A. Chemori and A. Loria, "Control of a planar underactuated biped on a complete walking cycle," IEEE Trans. Autom. Control **49**, 838–843 (2004).
19. Y. Aoustin and A. Formal'sky, "On the stabilization of a biped vertical posture in single support using internal torques," *Robotica* **23**, 65–74 (2005).
20. M. Nikkhah, H. Ashrafiuon and F. Fahimi, "Sliding Mode Control of Underactuated Biped Robots," *Proceedings of the ASME International Mechanical Engineering Congress and Exposition*, Orlando, FL (Nov. 2005) pp. 1283–1288.
21. M. W. Spong, "Underactuated Mechanical Systems," **In**: *Control Problems in Robotics and Automation* (B. Siciliano and K. P. Valavanis, eds.) (Springer-Verlag, London, 1998) pp. 135–150, LNCIS, vol. 230.
22. V. I. Utkin, "Variable structure systems with sliding modes," IEEE Trans. Autom. Control **22**, 212–222 (1977).
23. M. Reyhanoglu, A. van der Schaft, N. H. McClamroch and I. Kolmanovsky, "Dynamics and control of a class of underactuated mechanical systems," IEEE Trans. Autom. Control **44**, 1663–1671 (1999).
24. H. Ashrafiuon and R. S. Erwin, "Sliding Control Approach to Underactuated Multibody Systems," *Proceedings of the American Control Conference*, Boston, MA (Jun./Jul. 2004) pp. 1283–1288.
25. D. S. Bernstein, *Matrix Mathematics: Theory, Facts, and Formulas with Application to Linear Systems Theory* (Princeton University Press, Princeton, NJ, 2005).
26. J.-J. E. Slotine and W. Li, *Applied Nonlinear Control* (Prentice-Hall, Englewood Cliffs, NJ, 1991).
27. M. Nikkhah, H. Ashrafiuon and K. Muske, "Optimal Sliding Mode Control for Underactuated Systems," *Proceedings of the American Control Conference*, Minneapolis, MN (Jun. 2006) pp. 4688–4693.

https://doi.org/10.1017/S0263574706003183 Published online by Cambridge University Press